Micro–Computed Tomography–Guided Artificial Intelligence for Pulp Cavity and Tooth Segmentation on Cone-beam Computed Tomography

Xiang Lin, MSc,[*] Yujie Fu, PhD,[*] Genqiang Ren, MSc,[†] Xiaoyu Yang, MSc,[†] Wei Duan, MSc,[†] Yufei Chen, PhD,[†] and Qi Zhang, MD, PhD[*]

ABSTRACT

Introduction: This study proposes a novel data pipeline based on micro–computed tomographic (micro-CT) data for training the U-Net network to realize the automatic and accurate segmentation of the pulp cavity and tooth on cone-beam computed tomographic (CBCT) images. **Methods:** We collected CBCT data and micro-CT data of 30 teeth. CBCT data were processed and transformed into small field of view and high-resolution CBCT images of each tooth. Twenty-five sets were randomly assigned to the training set and the remaining 5 sets to the test set. We used 2 data pipelines for U-Net network training: one manually labeled by an endodontic specialist as the control group and one processed from the micro-CT data as the experimental group. The 3-dimensional models constructed using micro-CT data in the test set were taken as the ground truth. The Dice similarity coefficient, precision rate, recall rate, average symmetric surface distance, Hausdorff distance, and morphologic analysis were used for performance evaluation. **Results:** The segmentation accuracy of the experimental group measured by the Dice similarity coefficient, precision rate, recall rate, average symmetric surface distance, and Hausdorff distance were 96.20% ± 0.58%, 97.31% ± 0.38%, 95.11% ± 0.97%, 0.09 ± 0.01 mm, and 1.54 ± 0.51 mm in the tooth and 86.75% ± 2.42%, 84.45% ± 7.77%, 89.94% ± 4.56%, 0.08 ± 0.02 mm, and 1.99 ± 0.67 mm in the pulp cavity, respectively, which were better than the control group. Morphologic analysis suggested the segmentation results of the experimental group were better than those of the control group. **Conclusions:** This study proposed an automatic and accurate approach for tooth and pulp cavity segmentation on CBCT images, which can be applied in research and clinical tasks. *(J Endod 2021;47:1933–1941.)*

KEY WORDS

Data pipeline; micro–computed tomography; segmentation accuracy; tooth and pulp cavity segmentation; U-Net network

SIGNIFICANCE

The method proposed in this study realizes the automatic and accurate segmentation of the pulp cavity and tooth on cone-beam computed tomographic images, which can be applied in future image segmentation tasks of anatomy research, clinical diagnosis, and treatment plan design.

Radiographic imaging and interpretation are indispensable in endodontics to provide a basis for endodontic diagnosis and treatment[1]. With the advancement of radiographic technology, our understanding of endodontic diseases has increased. Cone-beam computed tomographic (CBCT) imaging was invented in the 1990s. It provides 3-dimensional (3D) information of the subject by a series of cross sections that are obtained by continuous projection with cone-beam X-rays and mathematical reconstruction[2]. The 3D information provided by CBCT imaging solves the problems of image overlap and distortion in the periapical radiograph and improves the sensitivity and specificity of clinical diagnosis[3–5]. Therefore, CBCT examination is essential for the diagnosis and treatment of complicated endodontic cases[6].

As therapy concepts and techniques continuously evolve, CBCT imaging can be used with specialized modeling software to build 3D models to assist endodontic diagnosis and treatment[7]. To date, several reports have described the contribution of CBCT 3D modeling in the diagnosis and treatment of complex endodontic cases. For example, 3D models have been used in the endodontic

From the *Department of Endodontics, School and Hospital of Stomatology, Tongji University, Shanghai Engineering Research Center of Tooth Restoration and Regeneration, Shanghai, China; and [†]College of Electronics and Information Engineering, Tongji University, Shanghai, China

Address requests for reprints to Dr Yufei Chen, College of Electronics and Information Engineering, Tongji University, Shanghai 201804, China, or Dr Qi Zhang, Department of Endodontics, School and Hospital of Stomatology, Tongji University, Shanghai Engineering Research Center of Tooth Restoration and Regeneration, Shanghai 200072, China.
E-mail addresses: yufeichen@tongji.edu.cn or qizhang@tongji.edu.cn
0099-2399/$ - see front matter

https://doi.org/10.1016/j.joen.2021.09.001

treatment of a complex type 3 dens invaginatus[8], an anomalous anterior tooth[9], and an upper premolar with pulp canal obliteration and apical periodontitis[10]. Segmentation is fundamental to medical image analysis and aims to locate regions of interest in an image[11]. Accurate segmentation in every CBCT slice determines the accuracy of the final 3D model. However, most of the reviewed cases suffered from the fact that the segmentation of 3D models was manually labeled, which was too time-consuming and laborious. In addition, the difficulties in learning and using 3D modeling software also limit the clinical application of this method. Thus, exploring automatic image recognition and segmentation methods is both necessary and meaningful[12].

In computer vision, automatic image segmentation is 1 of the most fundamental tasks. In recent years, artificial intelligence (AI) has made significant progress in the field of automatic image recognition[13]. Convolutional neural networks (CNNs) have become the most popular method for automatic image segmentation in medical imaging[14,15]. In the dental field, several studies have used CNNs to recognize the entire dentition[16,17], root[18], and pulp chamber[19] of the tooth. Our previous research proposed a 2-phase deep learning solution for automatic tooth and pulp cavity segmentation on CBCT images[20]. Although these studies have achieved good results, there is still a key problem regarding the manual labeling of specialists as the ground truth for neural network training and testing. It is well-known that the accuracy of manual labeling depends on the specialist's recognition of the medical images. Furthermore, because of limited radiation doses, CBCT imaging exhibits intrinsic limitations, including poor soft tissue contrast, intensity inhomogeneity, and image noise[21], leading to insufficient fine details of anatomic structures[22]. Thus, it is difficult for endodontic specialists to define the ambiguous boundaries of the root canal precisely, particularly in the apical third. Hence, in pulp cavity segmentation tasks, manual labeling has limitations in being used as the training sample and ground truth. It is necessary to seek a more reliable type of training sample and ground truth.

Micro-CT imaging is the most important and accurate tool for studying root canal systems *in vitro*[23]. It can provide images with micron-scale resolution and the possibility of 3D visualization and analysis of endodontic morphology[24]. Given the potential issues in CBCT imaging, it is worth attempting to combine the advantages of high precision in micro-CT images and the clinical applicability of CBCT imaging. Thus, if the *in vivo* CBCT data and *in vitro* micro-CT data of the same tooth are both collected, the micro-CT data will become a reliable source of the training samples and promising ground truth for CBCT image segmentation tasks.

This study aims to use a novel data pipeline based on micro-CT data to train the U-Net convolutional neural network for accurate pulp cavity and tooth segmentation on CBCT images. The Dice similarity coefficient (DSC), precision rate (PR), recall rate (RR), average symmetric surface distance (ASSD), Hausdorff distance (HD), and morphologic analyses were used to evaluate the performance of the proposed method.

MATERIALS AND METHODS

The Ethics Committee of the Affiliated Stomatology Hospital of Tongji University, Shanghai, China, approved this study ([2019]-R-79).

Acquisition of Isolated Teeth, CBCT Data, and Micro-CT Data

From December 2019 to December 2020, 30 teeth extracted for orthodontic reasons and their CBCT images were collected from the Department of Orthodontics and Oral and Maxillofacial Surgery, Affiliated Stomatology Hospital of Tongji University. These teeth were intact without any treatment before extraction and could be seen completely in the CBCT images without any artifacts. Digital radiographs were used to ensure these teeth met the following inclusion criteria: single-root first/second maxillary/mandibular premolars with fully formed apices and intact teeth without any restorations. All obtained CBCT data were under the principle of radiation dosage "as low as reasonably achievable" [6]. All the data were anonymized.

These data were obtained using a 3D Accuitomo CBCT machine (MCT-1[EX-2F]; J Morita Manufacturing Corp, Kyoto, Japan). The field of view was 14 cm × 14 cm × 10 cm, and the voxel size was 250 μm × 250 μm × 250 μm. According to the manufacturer's instructions, the exposure parameters were set as follows: voltage of 85 kV, current of 10 mA, and time of 17.5 seconds. Then, the volumes were transformed into a panoramic view and put into the region proposal network with a feature pyramid network proposed in our previous research[20] to locate the extracted tooth and obtain its bounding box (Fig. 1*A* and *B*). The voxel size of these extracted CBCT images was decreased to 100 μm × 100 μm × 100 μm by interpolation, and all boxes were unified to the same size of 128 × 128 × 256 pixels (Fig. 1*C*). These data were exported in the Digital Imaging and Communications in Medicine format.

All extracted teeth were cleaned using an ultrasonic scaler and stored in a vial containing 4% thymol blue solution. These teeth were scanned by the Scanco microCT 50 scanner (Scanco Medical, Bassersdorf, Switzerland) operated at 70 kV, 200 μA, and a resolution of 20 μm, resulting in 1200–1500 slices per tooth. A 0.5-mm-thick aluminum filter was used to reduce beam hardening. All data were exported in the Digital Imaging and Communications in Medicine format.

Acquisition of the Training Samples in the Control and Experimental Groups

In the control group, the tooth and pulp cavity on the processed CBCT images were labeled by an endodontic specialist in the Medical Imaging Interaction Toolkit Workbench software (version 2018.04.2, available from http://mitk.org), which were used as the training samples for subsequent experiments.

In the experimental group, the training samples were obtained by the following steps. First, an endodontic specialist labeled the tooth masks on CBCT images (Fig. 1*D*). These masks were used to construct a 3D tooth model without any pulp cavity (Fig. 1*E*). Meanwhile, another 3D tooth model with the pulp cavity was reconstructed by a technician performing threshold segmentation on micro-CT images of the same tooth in MIMICS 17.0 software (Materialise NV, Leuven, Belgium) (Fig. 1*F–H*). The threshold range was set at 3500–15,000 HU determined by endodontic specialists based on micro-CT images. Then, the surface registration of the 2 models was performed by the iterative closest point algorithm (Fig. 1*I*). In this way, the high-precision micro-CT 3D model with the pulp cavity was positioned on the CBCT images. Then, a surface-to-image function of the Medical Imaging Interaction Toolkit Workbench was conducted to map the 3D high-precision information of the micro-CT model on 2-dimensional CBCT images. Based on this information, we obtained precise training samples of the pulp cavity and tooth on CBCT images (Fig. 1*J*).

U-Net Neural Network Training and Testing

The U-Net neural network segmentation algorithm (Fig. 1*L*) we used was proposed in our previous study[20]. It is a 2-dimensional U-Net network, and the sagittal and axial slices were used for tooth and pulp cavity segmentation, respectively.

Thirty groups of preprocessed CBCT data were randomly divided into 25 groups as

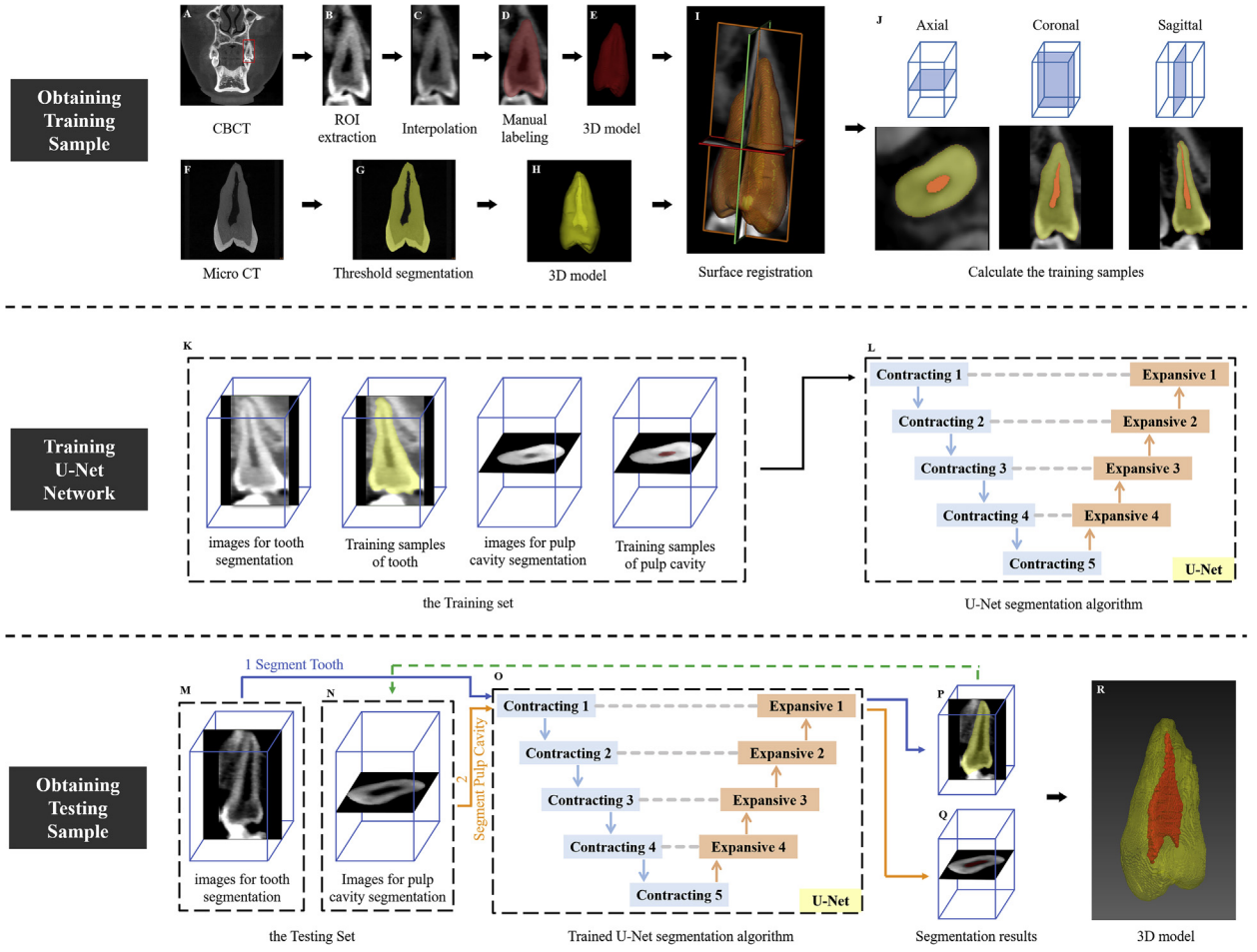

FIGURE 1 – The framework for tooth and pulp cavity segmentation in the experimental group. (*A*) The original CBCT images. (*B*) The region of interest (ROI) was extracted from the original CBCT image. (*C*) Using the interpolation to decrease the voxel size of the image to 100 μm^3. (*D*) The tooth was manually labeled. (*E*) The manually labeled tooth was constructed into a 3D model. (*F*) The original micro-CT images. (*G*) Using the threshold segmentation to segment the tooth and pulp cavity. (*H*) The result of the threshold segmentation was constructed to another 3D model. (*I*) The surface registration of the 2 models was performed by the iterative closest point algorithm. (*J*) The training samples were mapped based on the 3D micro-CT model. (*K*) The training data set, including the images and corresponding training samples of the tooth and pulp cavities. (*L*) The U-Net segmentation algorithm. (*M*) CBCT images were used for tooth segmentation. (*N*) Processed CBCT images used for pulp cavity segmentation. (*O*) The trained U-Net segmentation algorithm. (*P*) The segmentation results of the tooth. (*Q*) The segmentation results of the pulp cavity. (*R*) The result of segmentation was constructed to the final 3D model for testing.

the training set and the remaining 5 groups as the test set. Therefore, a total of 3200 sagittal slices and 6400 axial slices and corresponding training samples of the experimental and control groups were imported into the U-Net network segmentation algorithm for training (Fig. 1*K*). The network was implemented in PyTorch (version 1.7.0, available from https://pytorch.org) and trained on a server with NVIDIA Tesla P4 (NVIDIA, Santa Clara, CA, USA).

Then, the trained algorithms of the experimental and control groups were used to segment the tooth and pulp cavity on the CBCT images of the test set. The algorithm was iteratively performed for tooth and pulp cavity segmentation. Tooth segmentation was implemented first, and then the CBCT images within the range of the tooth segmentation results were extracted for pulp cavity segmentation (Fig. 1*M*–*Q*). Then, we constructed the 3D models based on the segmentation results as testing samples (Fig. 1*R*), and the pulp cavity models were divided into pulp chamber parts and root canal parts for further comparison. The 3D models constructed by micro-CT data in the test set were taken as the ground truth. There is a framework for tooth and pulp cavity segmentation in the experimental group (Fig. 1).

Performance Evaluation

Apart from the comparison of segmentation accuracy between the experimental group and the control group, we designed the other 3 comparison groups to evaluate the differences between the 2 types of training samples and the learning ability of our U-Net segmentation algorithm. Therefore, we collected the training samples and segmentation results of the experimental group and control group in the test set.

CG^{ts}/EG^{ts} Group

The training samples of the control group (CG^{ts}) were compared with those of the experimental group (EG^{ts}).

EG^{sr}/EG^{ts} Group

The segmentation results of the experimental group (EG^{sr}) were compared with matched training samples (EG^{ts}) to evaluate the segmentation accuracy of the algorithm.

CG^{sr}/CG^{ts} Group

The segmentation results of the control group (CG^{sr}) were compared with the matched training samples (CG^{ts}) to evaluate the learning ability of the algorithm.

Quantitative Analysis

To quantitatively evaluate the difference between the segmentation result and the ground truth, the DSC, PR, RR, ASSD, and HD were used as evaluation metrics as follows:

$$DSC = \frac{2 \times |M^{gt} \cap M^{sr}|}{|M^{gt}| + |M^{sr}|}$$

$$PR = \frac{|M^{gt} \cap M^{sr}|}{|M^{sr}|}$$

$$RR = \frac{|M^{gt} \cap M^{sr}|}{|M^{gt}|}$$

$$ASSD = \frac{\sum_{P^{sr} \varepsilon S^{sr}} D(P^{sr}, S^{gt}) + \sum_{P^{gt} \varepsilon S^{gt}} D(P^{gt}, S^{sr})}{|S^{sr}| + |S^{gt}|}$$

$$HD = max\left(\max_{P^{sr} \varepsilon S^{sr}} (D(P^{sr}, S^{gt})), \max_{P^{gt} \varepsilon S^{gt}} (D(P^{gt}, S^{sr})) \right)$$

M^{gt} is the ground truth, M^{sr} is the segmentation result, S^{gt} is the collection of surface points of the ground truth, S^{sr} represents the collection of surface points of the segmentation result, P^{gt} represents any point of the ground truth, P^{sr} represents any point of the segmentation result, and D(P, S) represents the Euclidean distance from the point to the surface.

The DSC value indicates the similarity between the segmentation result and the ground truth. The PR value indicates the degree of oversegmentation, and the RR value indicates the degree of undersegmentation. The ASSD value indicates the average surface deviation, and the HD value indicates the maximum surface deviation. Table 1 summarizes the evaluation results of the tooth, pulp cavity, pulp chamber, and root canal segmentation in the control and experimental groups.

Morphologic Differences Analysis

Geomagic Studio 2012 software (Geomagic, Durham, NC) was adopted to create a chromaticity diagram of the morphologic distribution difference between testing samples and the ground truth. This method allows visual evaluation of morphologic differences between the 2 models.

Statistical Analysis

All data are presented as the mean ± standard deviation. First, data were tested for normality (using the Shapiro-Wilk normality test). Then, appropriate statistical tests were implemented (1-sample *t* test for unpaired normally distributed data, paired *t* test for paired normally distributed data, the Mann-Whitney *U* test for unpaired nonparametric data, and Wilcoxon rank tests for paired nonparametric data). Statistical analyses were conducted using SPSS Statistics 20 (IBM, Armonk, NY), and statistical significance was set at $P < .05$.

RESULTS

Table 1 summarizes the performance for tooth, pulp cavity, pulp chamber, and root canal segmentation in the control and experimental groups. In the experimental group, the DSC of the tooth, pulp cavity, pulp chamber, and root canal were all significantly higher than those in the control group ($P < .05$) (Fig. 2*A*). The PR of the pulp chamber and the RR of the tooth and root canal in the experimental group were all higher than those in the control group and had a statistically significant difference ($P < .05$) (Fig. 2*B* and *C*). In addition, the ASSDs of the tooth, pulp cavity, pulp chamber, and root canal in the experimental group were all lower than those of the control group with statistical significance ($P < .05$) (Fig. 2*D*). Lastly, the HDs of the pulp cavity, pulp chamber, and root canal in the experimental group were significantly lower than those in the control group (Fig. 2*E*).

Table 2 shows the comparisons between 2 types of training samples and the performance of the learning ability of the U-Net algorithm. In the CG^{ts}/EG^{ts} group, the DSC, PR, RR, and HD had a statistically significant difference between the tooth and pulp cavity. The EG^{sr}/EG^{ts} group and CG^{sr}/CG^{ts} group were set to evaluate the learning ability of the algorithm. These evaluation metrics between the 2 groups in the tooth or pulp cavity were almost the same. Only the HD of the CG^{sr}/CG^{ts} group in the pulp cavity was significantly lower than that of the EG^{sr}/EG^{ts} group in the pulp cavity.

The 3D models of a representative set of data in the test set were reconstructed, including the ground truth and segmentation results in the experimental and control groups (Fig. 2*F*). Obviously, the segmentation results of the experimental group were better than those of the control group, especially the result of canal segmentation. In addition, morphologic difference analysis was performed on these models (Fig. 2*G*). The 3D models and morphologic difference analysis of the remaining data in the test set are shown in Supplemental Figure S1 (available online at www.jendodon.com). The results showed that the tooth segmentation results of the experimental and control groups were similar to the ground truth processed from the micro-CT images. The canal segmentation of the control group had undergone undersegmentation; the results of the experimental group recognized most root canals, but the finer parts of the root canal, such as the apical third, could not be well identified.

TABLE 1 - The Performance of Tooth, Pulp Cavity, Pulp Chamber, and Root Canal Segmentation in the Control Group (CG) and Experimental Group (EG)

	Group	DSC(%)	PR(%)	RR(%)	ASSD(mm)	HD(mm)
Tooth	CG	94.79 ± 0.42	96.61 ± 0.95	93.05 ± 1.09	0.12 ± 0.01	1.33 ± 0.65
	EG	96.20 ± 0.58*	97.31 ± 0.38	95.11 ± 0.97*	0.09 ± 0.01*	1.54 ± 0.51
Pulp cavity	CG	79.53 ± 3.41	75.25 ± 6.26	84.67 ± 2.39	0.14 ± 0.03	3.14 ± 1.09
	EG	86.75 ± 2.42*	84.45 ± 7.77	89.94 ± 4.56	0.08 ± 0.02*	1.99 ± 0.67*
Pulp chamber	CG	73.62 ± 4.05	59.79 ± 6.03	96.61 ± 4.05	0.16 ± 0.02	0.69 ± 0.15
	EG	84.51 ± 2.02*	77.44 ± 5.18*	93.38 ± 3.03	0.09 ± 0.01*	048 ± 0.15*
Root canal	CG	81.87 ± 3.84	83.02 ± 7.64	81.14 ± 3.34	0.19 ± 0.03	3.14 ± 1.09
	EG	87.49 ± 3.32*	87.32 ± 10.55	88.96 ± 6.13*	0.10 ± 0.03*	1.99 ± 0.67*

ASSD, average symmetric surface distance; DSC, Dice similarity coefficient; HD, Hausdorff distance; PR, precision rate; RR, recall rate.
The data of the tooth, pulp cavity, pulp chamber, and root canal were analyzed separately.
*$P < .05$ (experimental group vs control group).

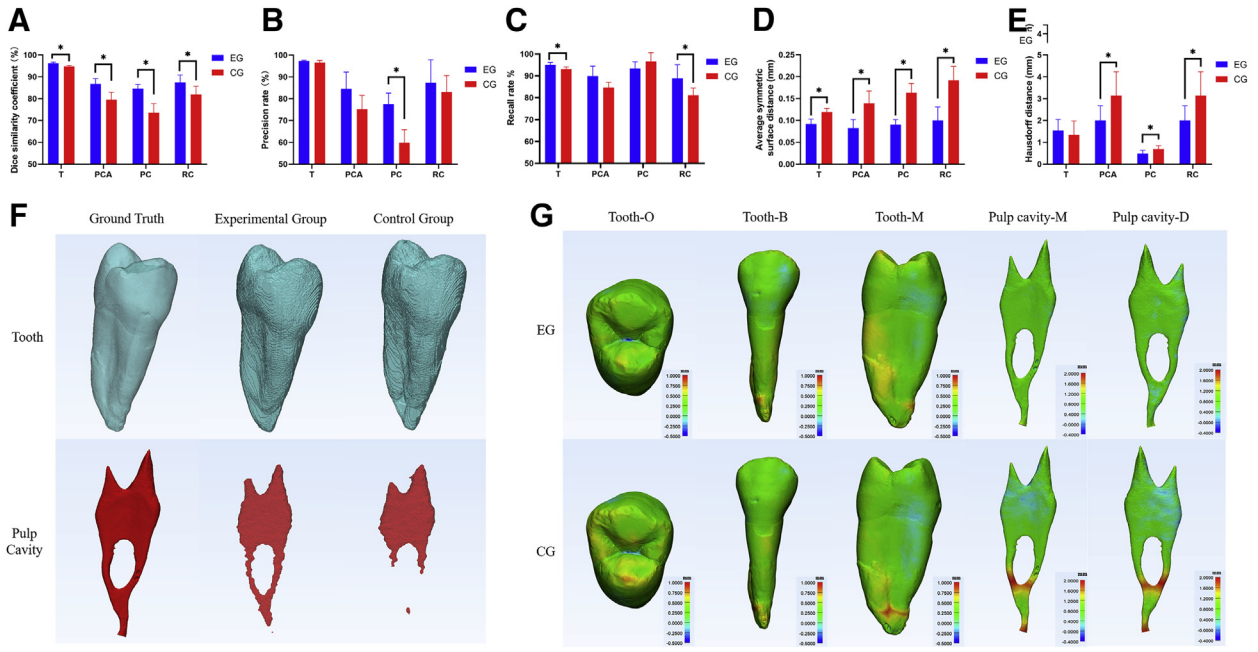

FIGURE 2 – The results of quantitative analysis and morphologic differences analysis in the experimental and control groups. (*A–E*) The DSC, PR, RR, ASSD, and HD comparison in the tooth, pulp cavity, pulp chamber, and root canal segmentation. T, tooth; PCA, pulp cavity; PC, pulp chamber; RC, root canal. *$P < .05$. (*F*) The 3D models of the tooth and pulp cavity reconstructed by the ground truth and the segmentation results of the experimental and control group on a representative CBCT data of the test set. (*G*) The chromaticity diagram of the difference in the morphologic distribution of a representative set of data in the test set. The color represents the Euclidean distance from the surfaces of the segmentation result to the ground truth. Blue and red represent the oversegmented and undersegmented parts of the segmentation results, respectively. O, occlusal surface; B, buccal surface; M, mesial surface; D, distal surface; EG, experimental group; CG, control group.

DISCUSSION

Tooth segmentation of CBCT images has been an area of growing interest. The development of AI has prompted researchers to construct more and more advanced tooth segmentation models to achieve accurate tooth segmentation. However, providing high-quality training samples for AI segmentation models has been less of a focus. This field in dental research is of concern and warrants further research.

It is generally known that teeth are hard tissues and are stable *in vivo* and *in vitro*. Micro-CT imaging is the most accurate tool for the study of tooth anatomy *in vitro*. Thus, micro-CT data of the tooth has the potential to become an excellent training sample for AI segmentation models to achieve accurate tooth and pulp cavity segmentation on CBCT images. Besides, in some studies, the 3D model based on micro-CT data through surface registration was used as the evaluation standard for CBCT tooth segmentation results[25,26]. This makes it possible to transform micro-CT data into the training samples for the neural network. Thus, we collected both *in vivo* CBCT and *in vitro* micro-CT images of the same tooth. We built an accurate 3D model of micro-CT data with the pulp cavity and located it on the paired CBCT images by surface registration. Then, the training sample of the tooth and the pulp cavity based on micro-CT data were calculated for subsequent training (Fig. 3*A–E*).

Compared with manual labeling, this method avoids individual image recognition differences and provides accurate training samples for neural networks. Even small root canals that are difficult for specialists to distinguish on CBCT images can be well labeled. Meanwhile, we used interpolation to refine the voxel size of the original CBCT images. This could solve the problem that some small root canals cannot be recognized because of the large voxels on the original CBCT image and make the edges of the segmentation results more coherent for a more

TABLE 2 - The Comparisons between 2 Types of Training Samples and the Performance of Learning Ability of the U-Net Algorithm

	Group	DSC (%)	PR (%)	RR (%)	ASSD (mm)	HD (mm)
Tooth	CG^{ts}/EG^{ts}	94.75 ± 1.01	93.29 ± 1.64	96.28 ± 1.67	0.11 ± 0.02	0.97 ± 0.52
	EG^{sr}/EG^{ts}	95.93 ± 0.71	93.66 ± 1.11	98.32 ± 0.49	0.08 ± 0.01	1.19 ± 0.51
	CG^{sr}/CG^{ts}	96.40 ± 0.52	94.95 ± 0.98	97.92 ± 0.98	0.07 ± 0.01	0.58 ± 0.12
Pulp cavity	CG^{ts}/EG^{ts}	83.12 ± 1.68*	84.97 ± 7.47*	82.09 ± 5.40*	0.10 ± 0.03	2.52 ± 0.79*
	EG^{sr}/EG^{ts}	88.96 ± 0.74	86.30 ± 4.68	92.14 ± 3.74	0.06 ± 0.01	1.87 ± 0.73
	CG^{sr}/CG^{ts}	90.10 ± 6.36	90.72 ± 3.68	90.78 ± 13.47	0.05 ± 0.03	0.97 ± 0.62†

ASSD, average symmetric surface distance; CG, control group; DSC, Dice similarity coefficient; EG, experimental group; HD, Hausdorff distance; sr, segmentation result; ts, training sample.

*$P < .05$ (tooth in the CG^{ts}/EG^{ts} group vs pulp in the CG^{ts}/EG^{ts} group).

†$P < .05$ (the EG^{sr}/EG^{ts} group vs the CG^{sr}/CG^{ts} group).

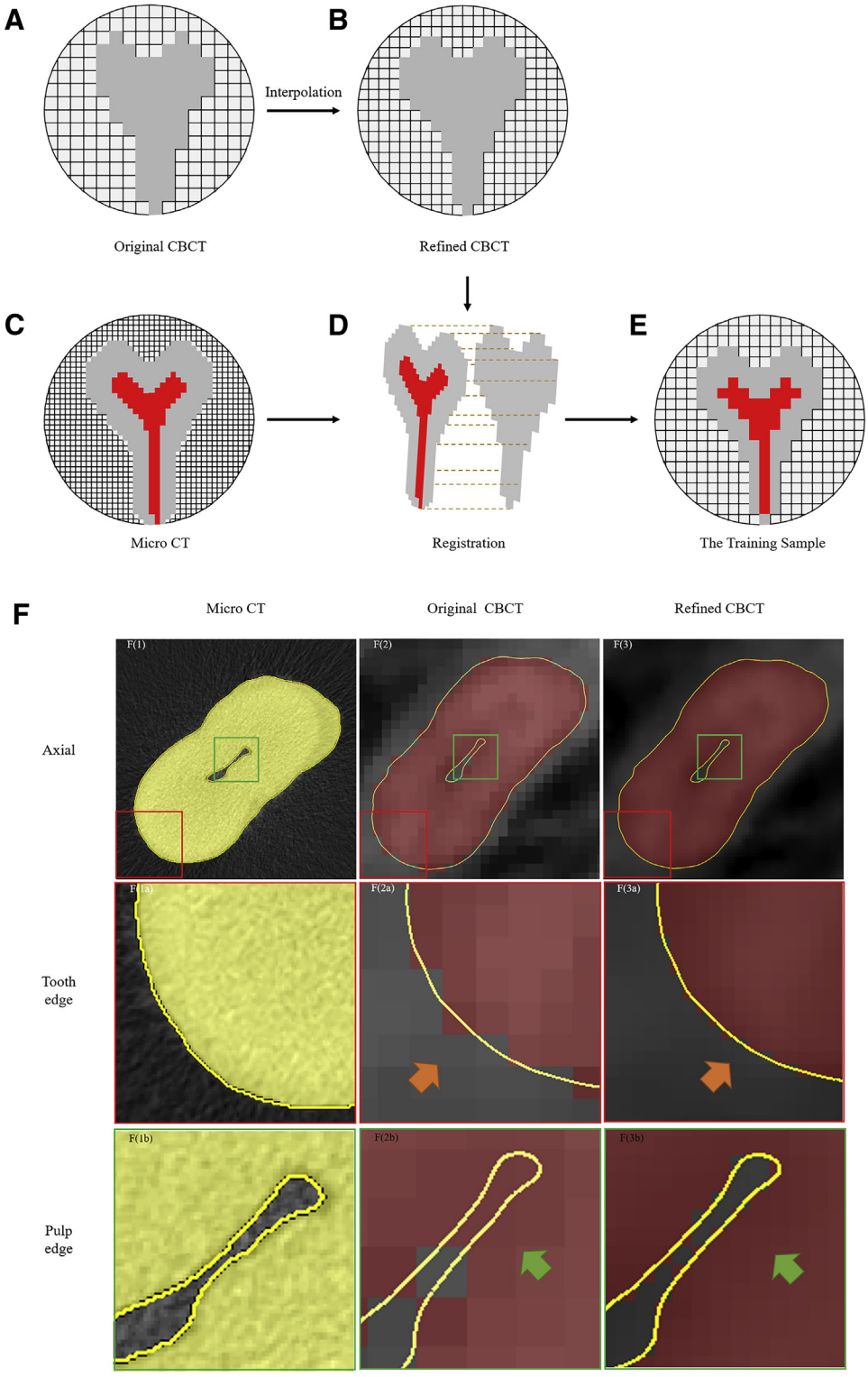

FIGURE 3 – The schematic diagram of registration and the reasons for image interpolation. (*A*) The gray voxels represented the tooth on the original CBCT image. (*B*) After the interpolation, the voxels on the original CBCT image became smaller, which showed more details. The gray voxels represented the tooth on the refined CBCT image. (C) In the micro-CT image, the gray voxels represented the tooth, and the red ones represented the pulp cavity. (*D*) After tooth surface registration, the layer information of the micro-CT image was located on the CBCT image at the same position. (*E*) Based on the information of the micro-CT image, the voxel sets representing the tooth and the pulp cavity on the refined CBCT image were calculated, which were used as the training sample. (*F*) *F(1)–F(3)* showed 1 layer image of the micro-CT image and its calculation results on the original CBCT image and the refined CBCT image. *F(1a)–F(3b)* showed the differences in calculation results between the original CBCT image and the refined CBCT image in the tooth edge and the pulp edge.

accurate segmentation result (Fig. 3*F*). In summary, the method proposed in this study combines the advantages of high precision in micro-CT images and the clinical applicability of CBCT imaging by the voxel refinement of the original CBCT images and mapping of the registered 3D micro-CT models. In addition, the neural network segmentation model trained in this way could be expected to enhance the image details of the original CBCT images in the future.

We chose sagittal and axial slices for tooth and pulp cavity segmentation, respectively, because of the result of the preliminary experiment (Supplemental Table S1 is available online at www.jendodon.com). The preliminary experiment included 20 groups of data and was designed using 10-fold cross-validation to compare the segmentation results of different CBCT views used for training the U-Net network segmentation algorithm. In the tooth group, the PR of sagittal views was significantly higher than that of coronal and axial views. In the pulp cavity, there was no statistical difference in the results from different views. Hence, we chose the axial view because it had the most slices.

According to the results of CG^{ts}/EG^{ts} group, we found that the training sample for tooth segmentation labeled by the specialist was very similar to those from micro-CT data. However, the comparison results for the pulp cavity had a certain degree of deviation. This may be attributable to the fact that the DSC, PR, and RR are related to the volume of the comparison object. Because the volume of the pulp cavity is smaller than that of the tooth, the same wrong segmentation (there was no statistical difference in ASSD between the tooth and pulp cavity in the CG^{ts}/EG^{ts} group) would cause these metrics of the pulp cavity to be more affected. However, it partly reflected that the pulp cavity on CBCT images was difficult to be fully distinguished by the endodontic specialist, which could also be inferred from the fact that the HD of the pulp cavity was significantly higher than that of teeth in the CG^{ts}/EG^{ts} group. Besides, the results of the EG^{sr}/EG^{ts} group and the CG^{sr}/CG^{ts} group in Table 2 indicate that the U-Net segmentation model we used had a good learning effect and stable learning performance. Under the experimental conditions of this study, irrespective of the training sample used, the difference between the segmentation results and the training samples was almost the same. The DSC of the U-Net model can reach 0.96 on tooth segmentation and 0.89 on pulp cavity segmentation. Compared with the existing research results on tooth segmentation, the DSC of the refined AI-driven segmentation algorithm [27] was 0.88 and that of the ToothNet segmentation algorithm[16] was 0.92. In addition, both quantitative analysis and morphologic difference analysis reflected that our proposed method performed significantly better than the previous manual labeling method (Fig. 2). In particular, for pulp cavity segmentation, the segmentation results were encouraging. Compared with the control group, the experimental group had a higher PR in the pulp chamber and a higher RR in the root canal, indicating that the U-Net trained by the training samples from micro-CT data achieved better pulp cavity segmentation by reducing oversegmentation of the pulp chamber and undersegmentation of the root canal. However, the results of the morphologic analysis suggested that the method proposed in our study still needs further research on the segmentation of finer root canals, such as the apical root canal (Fig. 2*G*).

Segmentation of the pulp cavity on CBCT images has always been a great challenge. Because of the limited spatial resolution of CBCT images, its ability to present small anatomic structures is insufficient. Coupled with the low contrast and unevenness of the images, the boundaries of the pulp cavity, especially the root canal, on the images are blurred. To date, few attempts at pulp cavity segmentation on CBCT images have been reported. Wang et al[28] proposed a simple threshold-based approach for pulp cavity segmentation, which could not guarantee an accurate and robust result and required manual selection of a single tooth region for subsequent processing. Zheng et al[19] used a coarse to fine strategy by integrating deep learning and a level set to segment the pulp chamber, but this research did not involve the segmentation of the root canal, and manual labeling was also taken as the ground truth, as in our previous research [20]. After we used the training samples from the micro-CT data, the DSC of the pulp cavity in the single-root tooth group reached 86.75% (±2.42%), and the ASSD was 0.08 mm (±0.02 mm), which showed the good performance and convincing segmentation results of the proposed method.

In recent years, there have been many publications and studies on the application of 3D models reconstructed from CBCT imaging, including anatomic research[29,30], guided endodontics[31], making 3-dimensional–printed teeth[32,33], and assisting clinical diagnosis and treatment[8]. The method proposed in this study could make the process of obtaining the 3D tooth and pulp cavity models based on CBCT images more automated and accurate. This will greatly expand the application prospects of 3D models reconstructed from CBCT imaging in the clinical diagnosis and treatment of endodontics. This study is a preliminary exploration of combining the advantages of high precision in micro-CT images and the clinical applicability of CBCT imaging. This kind of cross-modal information integration research can provide a more accurate imaging tool for clinical studies and will contribute to solving some clinical problems that cannot be solved by existing equipment in the future.

Nonetheless, the study has several limitations. For example, under the conditions of this study, only single-root premolars were collected for the experiment. Further investigations are required for teeth with more complex anatomic structures such as molars. The collected teeth were completely isolated. Future research needs to focus on endodontic diseases such as root fracture and calcified root canals to provide valuable insights for diagnosis and treatment and influence clinical decision making.

CONCLUSION

This study proposed a novel data pipeline based on micro-CT data that can be used to improve the segmentation accuracy of the U-Net segmentation model for tooth and pulp cavity on CBCT images. The 3D reconstruction models based on the segmentation results of the proposed method may greatly contribute to AI-driven applications in improving the accuracy and efficiency of endodontic diagnosis and therapy in the future.

ACKNOWLEDGMENTS

Xiang Lin and Yujie Fu contributed equally to this study.

Supported by the National Natural Science Foundation of China (grant no. 81870760), the Clinical Research Plan of Shanghai Hospital Development Center (grant no. SHDC2020CR3058B), the Shanghai Municipal Health Commission (grant no. 202040282), and the Fundamental Research Funds for the Central Universities (grant no. 22120190217).

The authors deny any conflicts of interest related to this study.

SUPPLEMENTARY MATERIAL

Supplementary material associated with this article can be found in the online version at www.jendodon.com (https://doi.org/10.1016/j.joen.2021.09.001).

REFERENCES

1. Kfir A, Basrani B. General principles of radiology in endodontics. In: Basrani B, editor. *Endodontic Radiology*. 2nd ed. Hoboken, NJ: John Wiley & Sons Inc; 2012. p. 1–17.
2. Pauwels R, Araki K, Siewerdsen J, et al. Technical aspects of dental CBCT: state of the art. Dentomaxillofac Radiol 2015;44:20140224.
3. Kruse C, Spin-Neto R, Wenzel A, et al. Cone beam computed tomography and periapical lesions: a systematic review analysing studies on diagnostic efficacy by a hierarchical model. Int Endod J 2015;48:815–28.
4. Patel S, Brown J, Pimentel T, et al. Cone beam computed tomography in Endodontics - a review of the literature. Int Endod J 2019;52:1138–52.
5. Johari M, Esmaeili F, Andalib A, et al. Detection of vertical root fractures in intact and endodontically treated premolar teeth by designing a probabilistic neural network: an *ex vivo* study. Dentomaxillofac Radiol 2017;46:20160107.
6. AAE and AAOMR joint position statement: use of cone beam computed tomography in endodontics 2015 update. Oral Surg Oral Med Oral Pathol Oral Radiol 2015;120:508–12.
7. van der Meer WJ, Vissink A, Ng YL, et al. 3D computer aided treatment planning in endodontics. J Dent 2016;45:67–72.
8. Kfir A, Telishevsky-Strauss Y, Leitner A, et al. The diagnosis and conservative treatment of a complex type 3 dens invaginatus using cone beam computed tomography (CBCT) and 3D plastic models. Int Endod J 2013;46:275–88.
9. Byun C, Kim C, Cho S, et al. Endodontic treatment of an anomalous anterior tooth with the aid of a 3-dimensional printed physical tooth model. J Endod 2015;41:961–5.
10. Torres A, Lerut K, Lambrechts P, et al. Guided endodontics: use of a sleeveless guide system on an upper premolar with pulp canal obliteration and apical periodontitis. J Endod 2021;47:133–9.
11. Pham DL, Xu C, Prince JL. Current methods in medical image segmentation. Annu Rev Biomed Eng 2000;2:315–37.
12. Cardenas CE, Yang J, Anderson BM, et al. Advances in auto-segmentation. Semin Radiat Oncol 2019;29:185–97.
13. Harris M, Qi A, Jeagal L, et al. A systematic review of the diagnostic accuracy of artificial intelligence-based computer programs to analyze chest x-rays for pulmonary tuberculosis. PLoS One 2019;14:e0221339.
14. Litjens G, Kooi T, Bejnordi BE, et al. A survey on deep learning in medical image analysis. Med Image Anal 2017;42:60–88.
15. Ronneberger O, Fischer P, Brox T. U-net: convolutional networks for biomedical image segmentation. International Conference on Medical Image Computing and Computer-assisted Intervention. 2015. p. 234–41.
16. Cui Z, Li C, Wang W. ToothNet: automatic tooth instance segmentation and identification from cone beam CT images. 2019 IEEE/CVF Conference on Computer Vision and Pattern Recognition. 2019. p. 6361–70.
17. Gou M, Rao Y, Zhang M, et al. Automatic image annotation and deep learning for tooth CT image segmentation. International Conference on Image and Graphics. New York: Springer; 2019. p. 519–28.
18. Li Q, Chen K, Han L, et al. Automatic tooth roots segmentation of cone beam computed tomography image sequences using U-net and RNN. J Xray Sci Technol 2020;28:905–22.
19. Zheng Q, Ge Z, Du H, et al. Age estimation based on 3D pulp chamber segmentation of first molars from cone-beam–computed tomography by integrated deep learning and level set. Int J Legal Med 2021;135:365–73.
20. Duan W, Chen Y, Zhang Q, et al. Refined tooth and pulp segmentation using U-Net in CBCT image. Dentomaxillofac Radiol 2021;50:20200251.
21. Patel S, Durack C, Abella F, et al. Cone beam computed tomography in endodontics - a review. Int Endod J 2015;48:3–15.
22. Brüllmann D, Schulze RK. Spatial resolution in CBCT machines for dental/maxillofacial applications-what do we know today? Dentomaxillofac Radiol 2015;44:20140204.
23. Aksoy U, Küçük M, Versiani MA, et al. Publication trends in micro-CT endodontic research: a bibliometric analysis over a 25-year period. Int Endod J 2021;54:343–53.

24. Wolf TG, Stiebritz M, Boemke N, et al. 3-dimensional analysis and literature review of the root canal morphology and physiological foramen geometry of 125 mandibular incisors by means of micro-computed tomography in a German population. J Endod 2020;46:184–91.

25. Michetti J, Basarab A, Diemer F, et al. Comparison of an adaptive local thresholding method on CBCT and μCT endodontic images. Phys Med Biol 2017;63:015020.

26. Galibourg A, Dumoncel J, Telmon N, et al. Assessment of automatic segmentation of teeth using a watershed-based method. Dentomaxillofac Radiol 2018;47:20170220.

27. Lahoud P, EzEldeen M, Beznik T, et al. Artificial intelligence for fast and accurate 3-dimensional tooth segmentation on cone-beam computed tomography. J Endod 2021;47:827–35.

28. Wang L, Li JP, Ge ZP, et al. CBCT image based segmentation method for tooth pulp cavity region extraction. Dentomaxillofac Radiol 2019;48:20180236.

29. Fu Y, Deng Q, Xie Z, et al. Coronal root canal morphology of permanent two-rooted mandibular first molars with novel 3D measurements. Int Endod J 2020;53:167–75.

30. Kim Y, Roh BD, Shin Y, et al. Morphological characteristics and classification of mandibular first molars having 2 distal roots or canals: 3-dimensional biometric analysis using cone-beam computed tomography in a Korean population. J Endod 2018;44:46–50.

31. Zehnder MS, Connert T, Weiger R, et al. Guided endodontics: accuracy of a novel method for guided access cavity preparation and root canal location. Int Endod J 2016;49:966–72.

32. Connert T, Krug R, Eggmann F, et al. Guided endodontics versus conventional access cavity preparation: a comparative study on substance loss using 3-dimensional-printed teeth. J Endod 2019;45:327–31.

33. Liang X, Liao W, Cai H, et al. 3D-printed artificial teeth: accuracy and application in root canal therapy. J Biomed Nanotechnol 2018;14:1477–85.